

Halo-independent tests of dark matter direct detection signals: local DM density, LHC, and thermal freeze-out

Mattias Blennow,^a Juan Herrero-Garcia,^a Thomas Schwetz^b and Stefan Vogl^b

^aDepartment of Theoretical Physics, School of Engineering Sciences, KTH Royal Institute of Technology, AlbaNova University Center, 106 91 Stockholm, Sweden

^bOskar Klein Centre for Cosmoparticle Physics, Department of Physics, Stockholm University, SE-10691 Stockholm, Sweden

E-mail: emb@kth.se, juhg@kth.se, schwetz@fysik.su.se, stefan.vogl@fysik.su.se

Abstract. From an assumed signal in a Dark Matter (DM) direct detection experiment a lower bound on the product of the DM–nucleon scattering cross section and the local DM density is derived, which is independent of the local DM velocity distribution. This can be combined with astrophysical determinations of the local DM density. Within a given particle physics model the bound also allows a robust comparison of a direct detection signal with limits from the LHC. Furthermore, the bound can be used to formulate a condition which has to be fulfilled if the particle responsible for the direct detection signal is a thermal relic, regardless of whether it constitutes all DM or only part of it. We illustrate the arguments by adopting a simplified DM model with a Z' mediator and assuming a signal in a future xenon direct detection experiment.

Keywords: dark matter theory, dark matter experiments, LHC

Contents

1	Introduction	1
2	Dark matter direct detection	2
3	Bounding the halo integral	4
4	A velocity-distribution-independent lower bound on $\rho_\chi\sigma_{\text{SI/SD}}$ from a direct detection signal	5
4.1	Lower bound from the number of observed events	6
4.2	Lower bound from a precise recoil energy spectrum measurement	8
4.3	Mock data for a possible DD signal	9
5	Comparison of a direct detection signal with LHC limits	11
6	Confronting a direct detection signal with the thermal freeze-out hypothesis	13
7	Discussion and conclusions	16

1 Introduction

We know from gravitational effects that dark matter (DM) constitutes a significant fraction of the energy density in the universe. One of the most promising ways to directly detect it is to look for the scattering of DM particles from the galactic halo in underground detectors [1–3]. In the interpretation of these direct detection (DD) signals, the astrophysical input plays a crucial role. Typically, the velocity distribution of DM is assumed to be a Maxwellian distribution truncated at the galactic escape velocity, v_{esc} , known as the Standard Halo Model (SHM). For a given halo model and a particle physics model for the DM–nucleus interaction, a positive direct detection signal will provide an allowed region in the dark matter mass (m_χ) vs. cross section plane ($\sigma_{\text{SI/SD}}$). However, using the SHM is very likely an oversimplification, with N -body simulations indicating a more complicated structure of the DM halo, see for instance refs. [4–6].

Therefore, in order to interpret DD signals, halo model independent methods have been developed [7–27]. Most of these use the fact that for a given particle physics model one can compare the results of different direct detection experiments without the need of specifying the total scattering cross section, the local DM density, the galactic escape velocity, nor the velocity distribution. In ref. [28] those methods have been extended to the comparison of a DD signal and a neutrino signal from DM annihilation inside the Sun. In the present paper we show how a positive signal from a DD detection experiment can be used to place a lower bound on the product of

the local DM density ρ_χ and the scattering cross section, independent of the DM velocity distribution. Within a given particle physics model such a lower bound can be compared to upper limits from LHC as well as to the hypothesis of DM production via thermal freeze-out in the early Universe.

This paper is structured as follows. After setting the notation for direct detection in sec. 2, we derive various inequalities involving the halo integral in sec. 3. In sec. 4 we apply those bounds to a positive signal in a direct detection experiment, leading to a lower bound on the product of the local DM density and the scattering cross section. Those bounds are independent of the DM velocity distribution, and we discuss various versions of the bound, highlighting the advantages and disadvantages of the different bounds in the case of the 3 DM candidate events observed in the CDMS experiment, as well as for mock data from a signal in a future direct detection experiment. In secs. 5 and 6 we adopt a so-called simplified DM model and show how the bounds from a DD experiment can be correlated with limits from LHC and with the thermal freeze-out hypothesis. We conclude in sec. 7.

2 Dark matter direct detection

In this section we review the relevant expressions for DD of dark matter. We focus on elastic scattering of DM particles χ with mass m_χ off a nucleus with mass number A and mass m_A , depositing the nuclear recoil energy E_R . The differential rate for a detector consisting of different target nuclei is given by:

$$\mathcal{R}(E_R, t) = \frac{\rho_\chi}{m_\chi} \sum_A \frac{f_A}{m_A} \int_{|\vec{v}| > v_m^A} d^3v v f_{\text{det}}(\vec{v}, t) \frac{d\sigma_A}{dE_R}(v), \quad (2.1)$$

where ρ_χ is the local DM mass density, f_A corresponds to the mass fraction of nuclei A in the detector, and

$$v_m^A = \sqrt{\frac{m_A E_R}{2\mu_{\chi A}^2}} \quad (2.2)$$

is the minimal velocity of the DM particle required for a recoil energy E_R , where $\mu_{\chi A}$ is the reduced mass of the DM–nucleus system. For single target detectors, there is just one contribution and thus the sum over A is absent. The function $f_{\text{det}}(\vec{v}, t)$ describes the distribution of DM particle velocities in the detector rest frame, with the normalization $\int d^3v f_{\text{det}}(\vec{v}, t) = 1$. The velocity distributions in the rest frames of the detector, the Sun and the galaxy are related by $f_{\text{det}}(\vec{v}, t) = f_{\text{Sun}}(\vec{v} + \vec{v}_e(t)) = f_{\text{gal}}(\vec{v} + \vec{v}_s + \vec{v}_e(t))$, where $\vec{v}_e(t)$ is the velocity vector of the Earth relative to the Sun and \vec{v}_s is the velocity of the Sun relative to the galactic frame. In the following we are going to ignore the small time dependence of the event rate due to $\vec{v}_e(t)$ and work in the approximation of $f_{\text{det}}(\vec{v}) \approx f_{\text{gal}}(\vec{v} + \vec{v}_s)$ being constant in time.¹

¹Bounds similar to the ones presented below based on the annual modulation signal can be found in ref. [29].

To be specific, in the following we will concentrate on spin-independent (SI) and spin-dependent (SD) scattering from a contact interaction. This implies that the differential scattering cross section $d\sigma_A(v)/dE_R$ scales as $1/v^2$. For SI contact interactions with equal DM couplings to neutrons and protons the cross section becomes

$$\frac{d\sigma_A}{dE_R}(v) = \frac{m_A \sigma_{\text{SI}} A^2}{2\mu_{\chi p}^2 v^2} F_A^2(E_R), \quad (2.3)$$

where σ_{SI} is the total DM–proton scattering cross section at zero momentum transfer, $\mu_{\chi p}$ is the DM–proton reduced mass, and $F_A(E_R)$ is a nuclear form factor. For SD interactions a similar formula applies with a different form factor and no A^2 enhancement, with the zero-momentum DM–proton scattering cross section denoted by σ_{SD} .

The event rate can be written as

$$\mathcal{R}(E_R) = \mathcal{C} \sum_A f_A A^2 F_A^2(E_R) \eta(v_m^A), \quad (2.4)$$

where we have defined

$$\eta(v_m^A) \equiv \int_{v > v_m^A} d^3v \frac{f_{\text{det}}(\vec{v})}{v}, \quad \mathcal{C} \equiv \frac{\rho_\chi \sigma_{\text{SI}}}{2m_\chi \mu_{\chi p}^2}. \quad (2.5)$$

For a specific detector the number of DM induced events in an energy range between E_1 and E_2 is given by

$$N_{[E_1, E_2]} = M T \mathcal{C} \langle \eta(v_m^A) \rangle_{E_1}^{E_2}, \quad (2.6)$$

where M and T are the detector mass and exposure time, respectively, and we introduce the short-hand notation for energy integration and target nucleus weighted sum of a quantity $X(v_m^A)$ as

$$\langle X \rangle_{E_1}^{E_2} \equiv \sum_A f_A A^2 \int_0^\infty dE_R F_A^2(E_R) G_{[E_1, E_2]}^A(E_R) X, \quad (2.7)$$

where $G_{[E_1, E_2]}^A(E_R)$ is the detector response function describing the probability that a DM event with true recoil energy E_R is reconstructed in the energy interval $[E_1, E_2]$, including energy resolution, energy dependent efficiencies, and possibly also quenching factors.²

²Note that $\langle X \rangle_{E_1}^{E_2}$ is not an average. We use this notation to indicate energy integration and sum over targets.

3 Bounding the halo integral

An upper bound on the halo integral $\eta(v_m)$ defined in eq. (2.5) can be derived in the following way (see also ref. [26]):

$$\begin{aligned}\eta(v_m^A) &\equiv \int_{v>v_m^A} d^3v \frac{f_{\text{det}}(\vec{v})}{v} \\ &\leq \frac{1}{v_m^A} \int_{v>v_m^A} d^3v f_{\text{det}}(v) \\ &\leq \frac{1}{v_m^A}\end{aligned}\tag{3.1}$$

where in the last step we used that $\int_{v_m}^\infty H(v) dv \leq \int_0^\infty H(v) dv$ for any positive function $H(v) \geq 0$, and the normalization condition. While the inequality is completely general and holds for all possible velocity distributions it will be useful only if it is not very far from being saturated, or in other words, if the ratio between the true value of $\eta(v_m^A)$ and $1/v_m^A$ is not too small. In fig. 1 we show with solid curves the product $v_m\eta(v_m)$ for the SHM as well as for two cold DM stream examples. If this product is close to one the inequality (3.1) is saturated and if it is much smaller than one the bound is weak. For the SHM³ one can see that the lower bound is reasonably strong in the v_m range between 50 and 500 km s⁻¹ and gets weak for low and high v_m values. An important point one should keep in mind is that, at very low DM masses, the v_m values relevant for DD can be much larger than the expected escape velocities in the detector rest-frame, ~ 750 km s⁻¹ (there are large uncertainties, see for instance refs. [12, 13, 30]). The upper bound in eq. (3.1) is going to become weak in scenarios where the high-velocity tail is probed, e.g. for low dark matter masses or high thresholds.

For streams the bound gets strong for v_m close to the velocity of the stream in the detector frame. This is obvious from eq. (3.1) by approximating a DM stream by $f(\vec{v}) \propto \delta^3(\vec{v} - \vec{v}_{\text{stream}})$. In this approximation $v_m\eta(v_m)$ is a linear function rising up to 1 at $v_m = v_{\text{stream}}$. This behavior is visible in fig. 1. The curves do not rise up to 1 because of the finite velocity dispersion of 20 km/s assumed in the calculations.

In ref. [22] a lower bound on the DM cross section was derived based on a different inequality for the halo integral. Having DD experiments sensitive to the velocity range between v_1 and v_2 in mind, one obtains the inequality [22]

$$1 = \int_0^\infty dv \eta(v) \geq v_1\eta(v_1) + \int_{v_1}^{v_2} dv \eta(v),\tag{3.2}$$

where the first identity follows from the normalization of $f_{\text{det}}(\vec{v})$ and the inequality follows from the fact that $\eta(v)$ is a non-negative monotonously decreasing function of v . We observe that eq. (3.1) simply corresponds to the first term in eq. (3.2). The dotted curves in fig. 1 show the right-hand side of eq. (3.2). We find that, for high

³Here and in the following we adopt the following parameters for the SHM: we use a Maxwellian velocity distribution with the mean velocity $\bar{v} = 220$ km/s, truncated at the escape velocity of $v_{\text{esc}} = 550$ km/s.

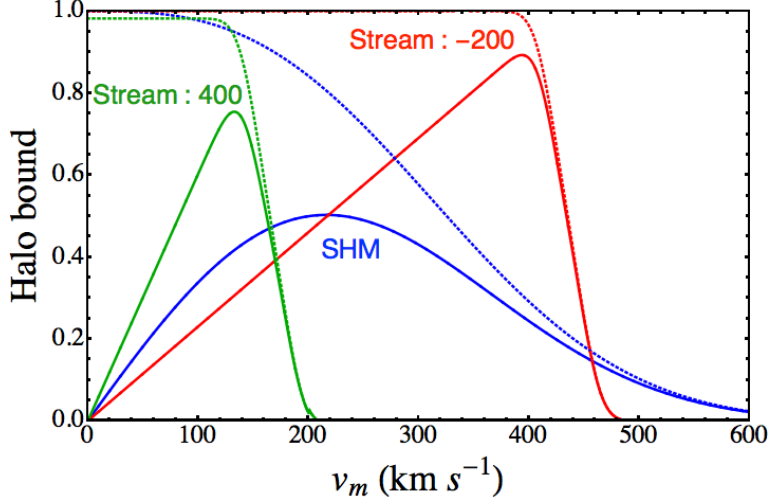


Figure 1. Strength of the bound on the halo integral versus v_m for the SHM (blue) and for two DM stream examples (red, green). We take the streams to be aligned with the motion of the Sun in the galaxy, where the velocities of the streams relative to the galaxy are chosen to be -200 (red) and $+400$ km/s (green), see labels in the plot. The velocity dispersion of the streams is taken to be 20 km/s. The solid curves show the product $v_m \eta(v_m)$, corresponding to the ratio of the left and right-hand sides of eq. (3.1). The dotted curves correspond to the right-hand side of eq. (3.2) with $v_1 = v_m$ and $v_2 \rightarrow \infty$.

velocities, the two bounds become similar, whereas for low velocities the inequality in eq. (3.2) is close to saturated and is expected to provide stronger bounds than eq. (3.1). Below we will comment on the advantages/disadvantages of the two bounds when applied to data.

Velocity distributions obtained from N-body simulations are qualitatively similar to the SHM, although quantitative differences occur, see e.g. [4–6]. Hence, the strength of the bounds for such velocity distributions is expected to be similar to the SHM case shown in fig. 1. Note also that a hypothetical dark matter disk effectively corresponds to a DM stream, and thus we expect also qualitatively a similar behaviour as for the streams shown in the figure.

4 A velocity-distribution-independent lower bound on $\rho_\chi \sigma_{\text{SI/SD}}$ from a direct detection signal

We now use the bounds on the halo integral to derive lower bounds on the product of DM density multiplied by the scattering cross section $\rho_\chi \sigma_{\text{SI/SD}}$. In sec. 4.1 we will use eq. (3.1) to derive a bound based on the number of observed events in a DD experiment, whereas in sec. 4.2 we will comment on a bound based on eq. (3.2), which is useful if the recoil energy spectrum of DM scattering events can be measured with high precision. In this section we concentrate on a signal from just one direct detection experiment, but we comment on the multi-experiment case in the conclusions, sec. 7.

4.1 Lower bound from the number of observed events

Let us now apply the bound eq. (3.1) to the event rate in a DD experiment. For definiteness we focus on SI interactions. The generalization to the SD case is straightforward. Inserting the bound from eq. (3.1) into eq. (2.4) we obtain

$$\mathcal{R}(E_R) \leq \mathcal{C} \sum_A \frac{f_A A^2 F_A^2(E_R)}{v_m^A(E_R)}. \quad (4.1)$$

With the definition of \mathcal{C} in eq. (2.5) this may be re-written as a lower bound on $\rho_\chi \sigma_{\text{SI}}$ which does not depend on $f(v)$:

$$\rho_\chi \sigma_{\text{SI}} \geq \frac{2 m_\chi \mu_{\chi p}^2}{\sum_A f_A A^2 F_A^2(E_R)/v_m^A(E_R)} \mathcal{R}(E_R). \quad (4.2)$$

This inequality must be fulfilled at all energies E_R . Taking the more realistic situation of a finite energy resolution and other detector effects into account we can also derive a corresponding bound in terms of the measured number of events within an energy interval $[E_1, E_2]$ by use of eq. (2.6):

$$\rho_\chi \sigma_{\text{SI}} \geq \frac{2 m_\chi \mu_{\chi p}^2}{MT \langle 1/v_m^A \rangle_{E_1}^{E_2}} N_{[E_1, E_2]}, \quad (4.3)$$

where $\langle 1/v_m^A \rangle_{E_1}^{E_2}$ is defined in eq. (2.7). If a DD experiment reports a lower bound B_{CL} at some confidence level (CL) on DM induced events in a certain energy interval, $N_{[E_1, E_2]} > B_{\text{CL}}$, then eq. (4.3) provides a lower bound on the product $\rho_\chi \sigma_{\text{SI}}$ at that CL, which is independent of the local DM velocity distribution.

In the following we use the putative signal from the CDMS silicon exposure [31] to illustrate how this bound can be used. The CDMS collaboration reports 3 candidate events from their data with a silicon target, rejecting the known-background-only hypothesis with a p -value of 0.19% when tested against the DM+background hypothesis using a profile likelihood ratio test. Although a DM interpretation of this signal is in tension with limits from other experiments [32–37] (see for instance refs. [22, 23] for halo-independent analyses) we use this signal as a case study and apply eq. (4.3) to it. We use the Helm parameterization for the SI form factor, $F(E_R) = 3e^{-q^2 s^2/2} [\sin(qr) - qr \cos(qr)] / (qr)^3$, with $q^2 = 2m_A E_R$, $s = 1$ fm, $r = \sqrt{R^2 - 5s^2}$ and $R = 1.2A^{1/3}$ fm.

The red curves in fig. 2 show the 90% CL lower bound on σ_{SI} from CDMS-Si data for a reference value of $\rho_\chi = 0.4 \text{ GeV/cm}^3$. Those can be compared to the allowed interval for σ_{SI} when the SHM is assumed (shown as blue shaded bands in the plot).⁴ The behavior follows from the discussion related to fig. 1. For low DM masses only large values of v_m are probed by the experiment and the bound becomes much weaker

⁴Note that the SHM region is based only on the observed number of events, without using any energy information. Therefore, we obtain a degenerate band in m_χ , opposed to the closed regions resulting e.g., from an event-based likelihood analysis.

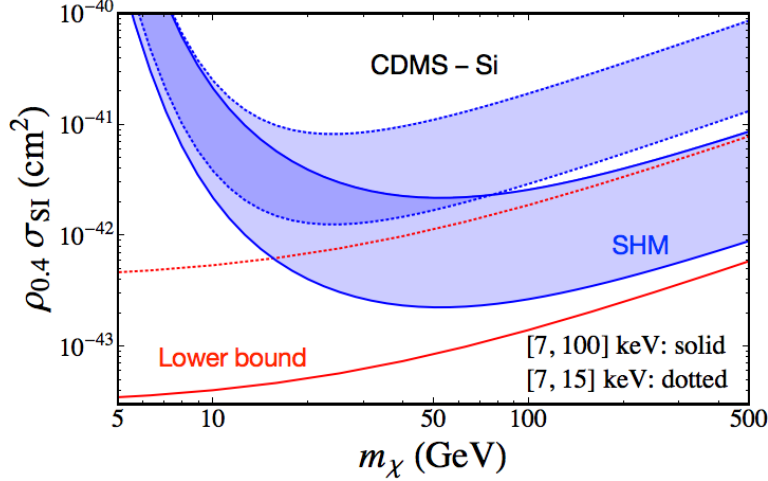


Figure 2. Lower bound (SHM interval) in red (blue) for $\rho_{0.4} \sigma_{\text{SI}}$ from CDMS-Si data versus DM mass, where $\rho_{0.4} \equiv \rho_\chi / (0.4 \text{ GeV cm}^{-3})$. We show the 90% CL results for two different choices of the energy range: [7, 15] keV (dotted) and [7, 100] keV (solid).

compared to the SHM, where no DM particles are left with such high velocities due to the escape velocity cut-off. For DM masses $m_\chi \gtrsim 100$ GeV the lower bound is close to the SHM interval. However, we note that for DM masses in that range the CDMS-Si signal is highly disfavoured by other experiments.

In general, for a given observed event distribution it is not a priori clear which energy interval will give the strongest constraint, as the expected spectrum $R_A(E_R)$ decreases with energy, while $v_m(E_R)$ increases. The form factor typically decreases, but can also show local minima. This effect is shown for CDMS-Si data in fig. 2, where the results are shown for two different energy intervals, [7, 15] keV and [7, 100] keV. We use the expected background spectrum from ref. [38]. We observe that the smaller energy interval, [7, 15] keV, provides the strongest bound, since in this case the signal to background ratio is highest.

Another way to use eq. (4.3) is to consider it as a lower bound on the local DM density ρ_χ for a given scattering cross section and DM mass. This lower bound can then be compared to astrophysical determinations of ρ_χ to identify regions in $\sigma_{\text{SI/SD}}$ and m_χ which are compatible with reasonable values of ρ_χ . In fig. 3, we show for illustration the 90% CL lower bound on the DM density from CDMS-Si data as a function of σ_{SI} for $m_\chi = 10$ GeV and compare it with the 90% CL interval obtained from assuming the SHM. We use the recoil energy interval of [7, 15] keV. The value for the DM chosen in the figure is motivated by the fact that typically for masses in this range the tension of the CDMS-Si signal with bounds from other experiments is less severe. Corresponding results for different dark matter masses can be obtained by recasting the limit on $\rho_{0.4} \sigma_{\text{SI}}$ shown in fig. 2 into the $(\sigma_{\text{SI}}, \rho_\chi)$ plane.

These results can be compared to astrophysical determinations of the local DM density. There are various methods to infer ρ_χ , either based on local dynamical tracers [39–41] or global methods based on fitting a mass model of the Milky Way to

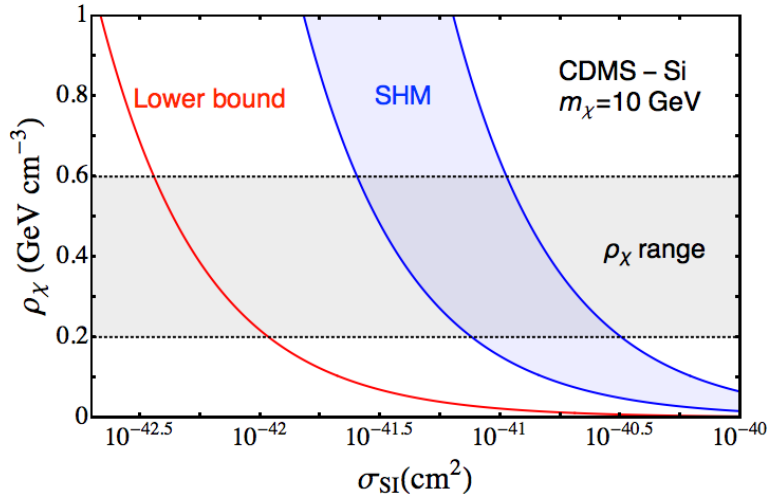


Figure 3. Lower bound at 90% CL on the local DM density ρ_χ from CDMS data (in red), shown for $m_\chi = 10$ GeV. The blue shaded region shows the allowed range at 90% CL assuming the SHM. The grey shaded horizontal band indicates the preferred range for ρ_χ from Milky Way observations.

observations [42–46] (see ref. [47] for a recent review). Depending on the different assumptions, values for ρ_χ roughly in the range between 0.2 and 0.6 GeV/cm³ are found, mostly consistent within the quoted error bars (with the size of the errors also strongly dependent on assumptions), see table 4 of ref. [47] for a summary. The gray shaded horizontal band in fig. 3 indicates the plausible range for ρ_χ , motivated by the studies quoted above. From the red curve in the figure we observe that cross sections of $\sigma_{\text{SD}} \lesssim 3 \times 10^{-43}$ cm² are disfavoured, since the local DM would need to be too high to obtain the observed signal for such small cross sections. Note that this argument also applies to the case when the species χ constitutes only part of the DM, since this would only increase the lower bound on the total DM density.

4.2 Lower bound from a precise recoil energy spectrum measurement

Let us now discuss a bound based on eq. (3.2). For a single target experiment with perfect energy resolution, a measurement of the spectrum $\mathcal{R}(E_R)$ allows a determination of the halo integral via eq. (2.4):

$$\eta(v_m^A) = \frac{\mathcal{R}(E_R)}{\mathcal{C} A^2 F_A^2(E_R)}. \quad (4.4)$$

Consider a spectral measurement of $\mathcal{R}(E_R)$ in the energy range $[E_1, E_2]$, which for a given DM mass can be related to a velocity interval $[v_1, v_2]$ via eq. (2.2). Inserting eq. (4.4) into the bound eq. (3.2) and using the definition of \mathcal{C} leads to the lower bound [22]

$$\rho_\chi \sigma_{\text{SI}} \geq \frac{2m_\chi \mu_{\chi p}^2}{A^2} \left(v_1 \frac{\mathcal{R}(E_1)}{F_A^2(E_1)} + \int_{v_1}^{v_2} dv \frac{\mathcal{R}(E_R)}{F_A^2(E_R)} \right), \quad (4.5)$$

where energies and velocities are related by eq. (2.2). In agreement with the discussion in sec. 3 we see that the first term on the right-hand side of eq. (4.5) agrees with eq. (4.2) in the limit of a single target.

In general, eq. (4.5) will lead to a stronger bound on $\rho_\chi \sigma_{\text{SI/SD}}$ than eq. (4.3). However, it requires a significantly more precise measurement. The spectrum $\mathcal{R}(E_R)$ has to be measured with high precision and all detector effects such as energy resolution and efficiencies have to be de-convoluted. Certainly this program cannot be carried out in the case of the 3 events from CDMS-Si, which we used above to illustrate the bound from eq. (4.3). In conclusion, the bound from eq. (4.5) is useful if a precision measurement of the DD event spectrum is available, while for low-statistics “discovery signals” the bound from eq. (4.3) can still be applied and gives a robust lower bound on $\rho_\chi \sigma_{\text{SI/SD}}$. Furthermore, the bound of eq. (4.3) can be applied to multi-target detectors, while that of eq. (4.5) cannot, as in general one cannot extract the different $\eta(v_m^A)$ from just one signal. Therefore, in those cases one needs to assume that a particular nuclei gives the dominant contribution. Let us proceed by comparing the two bounds in the case of a hypothetical future precision DD measurement.

4.3 Mock data for a possible DD signal

We introduce mock data for a possible future signal in a DD experiment, also in view of the discussion related to LHC following below. For SI interactions present limits from DD are so strong that constraints from LHC are typically not competitive, while for SD interactions LHC and DD are probing a similar region in parameter space. Therefore we will concentrate on SD interactions in this section. To generate mock data for a future DD signal we assume DM with $m_\chi = 150$ GeV and $\sigma_{\text{SD}}^p = \sigma_{\text{SD}}^n = 5 \cdot 10^{-41} \text{ cm}^2$, which is below the current limits [48–52] but should be observed in the not-too-far future. For SD interactions we take the nuclear structure functions from ref. [53].

As a representative example we consider a future xenon based experiment [54–56]. We adopt a threshold of 3 keV and take natural abundances of the isotopes with spin ^{129}Xe (26.4 %) and ^{131}Xe (21.2 %). We neglect the small mass difference between the two xenon isotopes, which implies that v_m and hence also $\eta(v_m)$ becomes independent of the isotope. We simulate mock data assuming the SHM (see footnote 3) and a local DM density $\rho_\chi = 0.4 \text{ GeV/cm}^3$. For an exposure of 1 ton yr at 100% efficiency and an energy resolution of 1 keV approximately 77 events would be observed in the energy range 3 – 45 keV. In the following analysis we compute the 90% CL lower bound in this energy range. Notice that we neglect a possible contamination with background and systematic errors. This idealized analysis suffices to illustrate the power of our bound. Once applied to real data an appropriate statistical analysis will have to be performed.

In fig. 4 we show the lower bounds on $\rho_\chi \sigma_{\text{SD}}$ resulting from this assumed DD signal, based on the bounds from eq. (4.3) (solid red), eq. (4.2) (dashed red), and eq. (4.5) (dotted red). These bounds can be compared to the region obtained from assuming the SHM (blue-shaded band). This region is obtained by simply fitting the total number of predicted events in the full energy range and is therefore a band degenerate in mass. This approach has been adopted in order to compare to the lower bound based on the

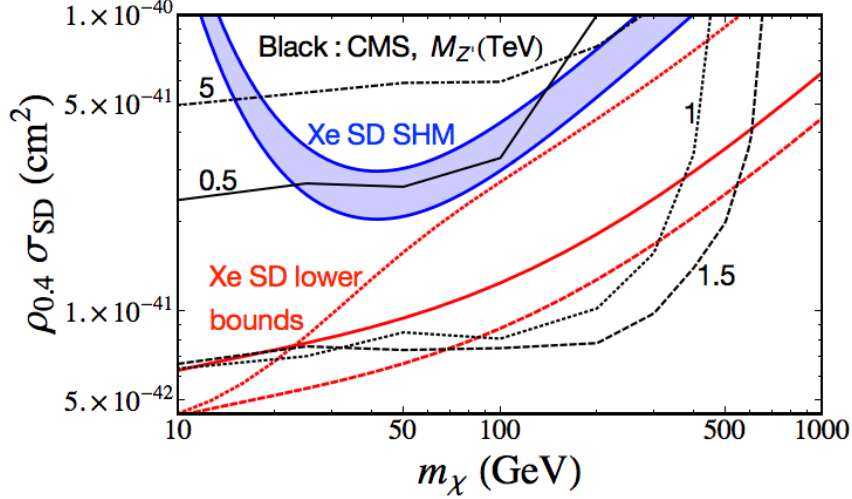


Figure 4. Red curves show the lower bound on $\rho_{0.4} \sigma_{SD}$ for the mock data generated for a xenon experiment, with $\rho_{0.4} \equiv \rho_\chi / (0.4 \text{ GeV cm}^{-3})$. The red solid, dashed and dotted curves correspond to the bounds from eqs. (4.3), (4.2), and (4.5), respectively. The blue-shaded region corresponds to the allowed range assuming the SHM. Black curves show upper limits from CMS at 95% CL assuming the simplified Majorana DM model for different masses of the Z' mediator (labels in the plot give $M_{Z'}$ in TeV).

same information. We note that if the SHM is assumed information on m_χ can be extracted by performing a spectral fit. In comparing the curves one should keep in mind that both the dotted and the dashed curves assume a perfect determination of the spectrum in an idealized experiment and correspond to the infinite-statistics limit. In contrast, the solid red curve and the blue region (SHM) show the 90% CL based on the statistical error from the 77 expected events.

By comparing the dashed and the dotted curves we appreciate the different strengths of the bounds based on eq. (3.1) and (3.2), respectively. We observe that they merge at low DM masses, in agreement with fig. 1, where, for large velocities (as relevant for small DM mass), the two bounds come close to each other and the bounds become weak in all cases. For masses $m_\chi \gtrsim 50 \text{ GeV}$ the limit from eq. (4.5) (based on (3.2)) [22] clearly becomes stronger than the one from eq. (4.2) (based on (3.1)), and comes relatively close to the “true” region. Again those features follow from the behavior shown in fig. 1. Note that both of those curves (dashed and dotted red) ignore effects of energy resolution and assume a perfect measurement of the spectrum $\mathcal{R}(E_R)$ at infinite precision (for the dashed curve we evaluate the bound of eq. (4.2) at the threshold of 3 keV).

The red solid curve corresponds to the bound from eq. (4.3) based on the total event rate in the full energy range, including also the finite energy resolution of 1 keV. The energy resolution is also the reason why this bound is stronger than the “ideal” bound from eq. (4.2) (dashed): because of the energy smearing events from below the threshold are reconstructed within the analysis window. This is a well-known effect, in particular in the context of the sensitivity to low-mass DM, and it turns out also to be

important for the bound discussed here. The reason why the slopes of the red dotted curve and the SHM region for $m_\chi \gtrsim 100$ GeV are slightly different is also the effect of the finite energy resolution. We have checked though, that all bounds as well as the SHM region become parallel for $m_\chi \gtrsim 1$ TeV, as expected from the $1/m_\chi$ dependence (irrespective of resolutions) in the limit of $m_\chi \gg m_A$.

5 Comparison of a direct detection signal with LHC limits

The comparison of a signal in a DD experiment with data from a collider experiment as well as the consideration of the hypothesis of a thermal history of the DM candidate necessarily depend on the particle physics model, since different particle reactions are relevant. In this section we adopt a specific simplified model for the DM candidate to illustrate how the halo bounds applied to a possible future DD signal can be used in the context of limits from LHC. In sec. 6, we will use the same simplified model to discuss a consistency check for the thermal freeze-out hypothesis.

In so-called simplified models for DM, a DM candidate particle (assumed to be stable) and a force mediator are added to the Standard Model, see refs. [57, 58] for a summary of the current status. As an example, we here adopt a simplified model with a Majorana fermion χ as the DM candidate, which interacts with the SM quarks q via a Z' boson with axial-vector couplings. The interaction Lagrangian of this model is

$$\mathcal{L}_{int} = g_\chi \bar{\chi} \gamma_\mu \gamma^5 \chi Z'^\mu + g_q \bar{q} \gamma_\mu \gamma^5 q Z'^\mu, \quad (5.1)$$

where g_χ and g_q are the strengths of the Z' interaction with the dark matter and light quarks, respectively. We assume equal couplings g_q to u, d, s, c quarks. Couplings to the third generation are irrelevant for DD (see below), and have little impact on LHC phenomenology (with the exception of on-shell production of the Z' , where the mono-jet rate depends on the partial widths of the Z' [59]). This simple framework suffices to discuss the phenomenology of interest to us; an extensive analysis of the model is beyond the scope of this work. Similar models have been considered recently for instance in refs. [59–63].

The spin-dependent scattering cross section is given by

$$\sigma_{SD}^N = \frac{12}{\pi} \frac{g_\chi^2}{M_{Z'}^4} \mu_{\chi p}^2 \left(\sum_q g_q \Delta_q^N \right)^2, \quad (5.2)$$

where N may denote a proton, p , or a neutron, n . The spin coefficients, which parametrize the contribution of the quark species q to the spin of the nucleon, are given by $\Delta_u^p = \Delta_d^n = 0.84$, $\Delta_d^p = \Delta_u^n = -0.43$ and $\Delta_s^{p,n} = -0.09$ [64]. Note that for our choice of equal couplings to quarks there will be a negative interference between the up and down quark contributions. Hence the scattering cross section is sensitive to the particular choice of g_q (including their relative signs).

Both ATLAS and CMS have obtained stringent limits on the interactions of dark matter with Standard Model (SM) particles based on monojet searches [65, 66]. Here,

we derive an upper limit on σ_{SD} from the 95% CL upper limit on anomalous monojet production reported by the CMS collaboration [66] based on 19.7 fb^{-1} collected at $\sqrt{s} = 8 \text{ TeV}$.⁵ MonteCarlo samples of the process $pp \rightarrow \chi\chi + \text{jet}$ generated with CalcHEP [67], are passed to Pythia [68] for hadronization before we simulate the effect of the CMS detector with Delphes [69]. As a cross check we have reproduced the CMS limits for dark matter interacting with quarks via effective operators. We find that the difference between our results and the official CMS limits, which can be seen as an estimate of the systematic uncertainty of our reinterpretation, is always smaller than 20%. For our CMS mono-jet analysis we keep the width of the Z' constant at a typical value for the considered parameter range. In general the width can be expected to influence the LHC limits. However, a full recast of the CMS search is beyond the scope of this work. In the fixed width approximation, LHC signatures depend only on the product of the couplings $g_\chi g_q$.

Note that within our assumption of equal couplings to light quarks, g_q can be pulled out of the sum in eq. (5.2) and σ_{SD} depends only on the product $g_\chi g_q$. Hence, for fixed DM and mediator masses, a DD signal provides a lower limit on $g_\chi g_q$, while LHC sets an upper limit on this quantity.

The black curves in Fig. 4 show the CMS limits on the Majorana fermion DM with axial interactions for different masses of the mediator (Z'). Comparing these upper limits with the lower bound from the assumed DD signal (e.g., red solid curve) we find that the interpretation of such a DD signal in terms of this model is in conflict with LHC null results for $M_{Z'} = 1 \sim 1.5 \text{ TeV}$, whereas a lighter or a heavier Z' could accommodate both results. We illustrate this behavior further in fig. 5, where we confront the interpretation of the direct detection signal using our velocity independent bound (red) or the SHM (in blue) together with the LHC. As can be seen, the LHC limits exclude a large portion of the parameter space in the $m_\chi - M_{Z'}$ plane independent of the velocity distribution. Furthermore, one has to take into account that in any sensible model the total width of the particles should be significantly smaller than their masses. We illustrate this in fig. 5, where above the dotted-dashed curves the DD signal implies that $\Gamma_{Z'} > M_{Z'}/2$. In this region the interpretation of the signal in terms of the simplified model is questionable and should be taken with caution.

For figs. 4 and 5 we have assumed $\rho_\chi = 0.4 \text{ GeV cm}^{-3}$. For different values of the local DM density the bounds from DD would shift, whereas the LHC limits would remain unaffected. Hence, the combined lower bound from DD and upper bound from LHC can be re-cast into a lower bound on the local DM density. This is shown in fig. 6 for a fixed DM mass of 100 GeV as a function of the Z' mass. The region in parameter space of the model where these limits are larger than allowed by astrophysical determinations of ρ_χ are excluded.⁶ Note that throughout this section we have compared an assumed future signal from a DD experiment with current LHC limits, while future limits are expected to increase the sensitivity by up to an order of magnitude [70].

⁵Additional constraints on the model coming from di-jet searches are discussed in ref. [59].

⁶The wiggles in the red and blue curves in fig. 6 are numerical artefacts related to the Monte Carlo statistics of the CMS detector simulation.

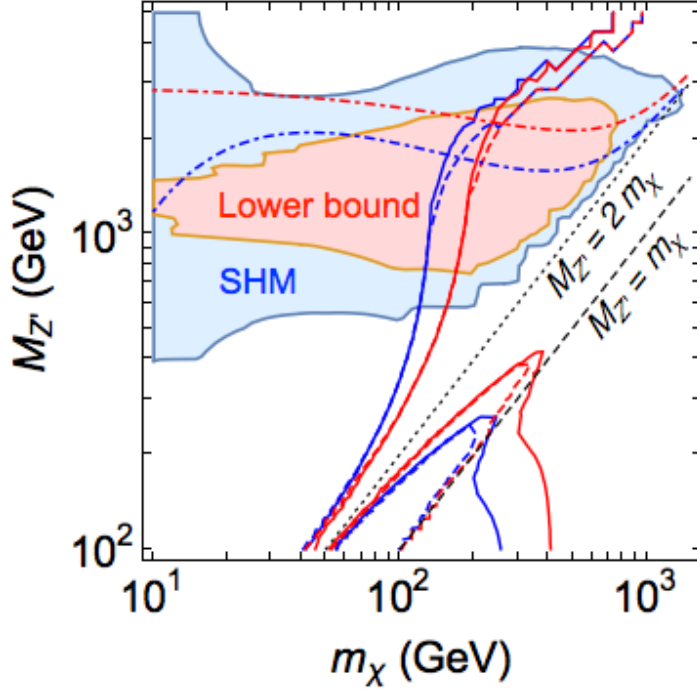


Figure 5. Constraints in the plane of DM (m_χ) and mediator ($M_{Z'}$) masses for the simplified DM model, eq. (5.1), assuming a DD signal in a future Xe experiment. The colored regions (blue for SHM, red for lower bound) inside the solid curves are excluded by comparing the CMS upper limits from mono-jet searches to DD data. To the right of the solid/dashed curves the DM candidate χ under consideration cannot be a thermal relic, where for the solid (dashed) curves we assume $g_\chi = g_q$ ($g_\chi = 10 g_q$). Above the dotted-dashed curves the DD signal can only be achieved if $\Gamma_{Z'} > M_{Z'}/2$. Red curves are based on the bound eq. (4.3) and blue ones assume the SHM. We take $\rho_\chi = 0.4 \text{ GeV/cm}^3$.

6 Confronting a direct detection signal with the thermal freeze-out hypothesis

Under the assumption that a DM candidate χ has been in thermal equilibrium with the plasma in the early Universe its relic abundance will be determined by the freeze-out of the $\chi\chi$ annihilation processes:⁷

$$\Omega_\chi h^2 \approx \Omega_{\text{tot}} h^2 \frac{\langle \sigma_{\text{th}} v \rangle}{\langle \sigma_{\chi\chi} v \rangle}, \quad (6.1)$$

where Ω_χ is the abundance of χ relative to the critical density of the Universe today, h parametrizes the Hubble constant, we use $\langle \sigma_{\chi\chi} v \rangle$ to denote the total annihilation cross section of χ times velocity, averaged over the thermal distribution in the early Universe,

⁷Notice that in the quantitative analysis at the end of this section we do not use the approximate relation from eq. (6.1), but we compute $\Omega_\chi h^2$ numerically using micrOMEGAs [71].

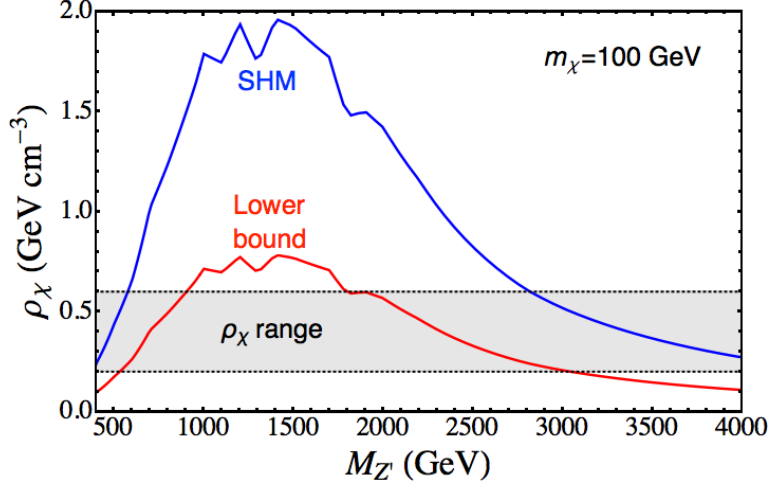


Figure 6. Lower bound on the local DM density ρ_χ from the combined lower bound on the scattering cross section from the DD mock data signal and the upper limits from CMS mono-jet searches within the simplified DM model. Lower bounds are shown as a function of the mediator mass for a fixed DM mass of 100 GeV. The red curve uses the velocity distribution independent lower bound from DD, whereas the blue curve assumes the SHM. The grey shaded horizontal band indicates the preferred range for ρ_χ from Milky Way observations.

and $\langle\sigma_{\text{th}}v\rangle \approx 3 \cdot 10^{-26} \text{ cm}^3 \text{ s}^{-1}$ is the annihilation cross section required to obtain the DM abundance as determined from cosmological observations [72], $\Omega_{\text{tot}} h^2 = 0.1194 \pm 0.0022$.

In a given particle physics model, the scattering cross section can be related to the annihilation cross section. Hence, under the thermal freeze-out hypothesis, a lower bound on $\rho_\chi \sigma_{\text{SI/SD}}$ will provide a lower bound on $\langle\sigma_{\chi\chi}v\rangle$ and therefore an upper bound on the relic density via eq. (6.1). For a given DM halo model this upper bound on the relic density becomes an equality. If this upper bound on the energy density is smaller than the value for Ω_{tot} determined from cosmological observations (or equivalently if the lower bound on $\langle\sigma_{\chi\chi}v\rangle$ is larger than $\langle\sigma_{\text{th}}v\rangle$), the observed direct detection rate is inconsistent with the thermal production of the DM candidate within a given model.

One might wonder whether it is possible to avoid this conclusion by allowing χ to become a subdominant component of DM. However, we would expect naively that a cosmological subdominant component of dark matter with $\Omega_\chi < \Omega_{\text{tot}}$ does not constitute all the dark matter locally and therefore $\rho_\chi < \rho_{\text{tot}}$. While a completely general statement is not possible we find that our bound can be extended to this case under certain conditions:

1. Only a single subdominant species χ induces the DD signal while more particles contribute to the DM in the universe (for instance well-known examples are axions or keV-scale sterile neutrinos).
2. The local density of χ in the galaxy is proportional to the global density:

$$\frac{\rho_\chi}{\rho_{\text{tot}}} = \frac{\Omega_\chi h^2}{\Omega_{\text{tot}} h^2}. \quad (6.2)$$

Eq. (6.2) assumes that all DM components contributing to structure formation are cold. In the presence of a cold/warm DM mix this assumption may be violated, see ref. [73] for a numerical study. Implications for the DD and LHC comparison under the proportional assumption of eq. (6.2) have been discussed previously in ref. [74].

Typically we expect $\langle\sigma_{\chi\chi}v\rangle \propto \sigma_{\text{SI/SD}}$, and, as the lower bound on $\sigma_{\text{SI/SD}}$ scales as $1/\rho_\chi$, see eq. (4.3), the upper bound on Ω_χ will be proportional to ρ_χ . Thus, if the upper bound on Ω_χ is smaller than Ω_{tot} for $\rho_\chi = \rho_{\text{tot}}$, eq. (6.2) implies that it will also be violated for any other value of $\Omega_\chi < \Omega_{\text{tot}}$ and $\rho_\chi < \rho_{\text{tot}}$. Hence, under these assumptions χ is inconsistent with having a thermal abundance, irrespective of whether it provides all of the DM or only part of it. This argument can be avoided by invoking some exotic physics which breaks the scaling relation in eq. (6.2) and enhances the local density of χ relative to the other DM species. The naive relic density approximation used in this discussion can be avoided by combining the lower bound of eq. (4.3) on $\rho_\chi \sigma_{\text{SI/SD}}$ directly with eq. (6.2). This yields a lower bound on $\Omega_\chi \sigma_{\text{SI/SD}}$ which is completely general and can be used within any given model even if Ω_χ , $\langle\sigma_{\chi\chi}v\rangle$ and $\sigma_{\text{SI/SD}}$ are not related by simple scaling relations or if higher precision is desired.

To illustrate the relic density bound numerically we adopt the DD mock data from sec. 4.3 and the Z' model from sec. 5. For calculating the relic density we use only the most minimal model able to provide a relevant scattering cross section, e.g., taking into account only Z' couplings to the light quarks (see sec. 5). If we allow for the possibility of additional annihilation channels (for instance into third generation quarks, leptons, or into hidden sector particles beyond the simplified model) the relic abundance can only become smaller.⁸ Hence, using the minimal model to calculate the upper bound on the relic abundance is conservative, as additional channels will make the inequality worse.

To the right of the solid or dashed curves in fig. 5, $\Omega_\chi = \Omega_{\text{tot}}$ is excluded where the red curve uses the bound from eq. (4.3) and the blue one assumes the SHM. In large part of the parameter space the bound is independent of the relative size of the coupling constants g_χ and g_q , since the relevant cross sections depend only on the product $g_\chi g_q$ (see below). To demonstrate this behavior explicitly we show the bound for $g_\chi = g_q$ (solid) and $g_\chi = 10 g_q$ (dashed).

For DM masses below the threshold for Z' pair production, i.e. for $M_{Z'} > m_\chi$, the annihilation cross section scales approximately as $\sigma_{\chi\chi}v \propto g_q^2 g_\chi^2 m_\chi^2 / (M_{Z'}^2 - 4m_\chi^2)^2$, while the scattering cross section from eq. (5.2) behaves as $\sigma_{\text{SD}} \propto g_q^2 g_\chi^2 m_p^2 / M_{Z'}^4$ (approximately independent of m_χ for $m_\chi \gg m_p$). In this regime both, $\sigma_{\chi\chi}v$ and σ_{SD} depend only on the product $g_\chi g_q$ and not on g_χ or g_q individually. This is apparent in the fig. 5, where for $M_{Z'} > 2m_\chi$ the curves for $g_\chi = g_q$ and $g_\chi = 10 g_q$ essentially overlap. Furthermore, since the bound scales approximately as $\sigma_{\text{SD}} / \langle\sigma_{\chi\chi}v\rangle$, it follows that it is independent of $g_\chi g_q$.

Near the resonance, $M_{Z'} \approx 2m_\chi$, the annihilation cross sections will be strongly enhanced for a given scattering cross section, and therefore for a given scattering cross

⁸This statement may not hold close to the resonance region, where additional channels lead to a larger width, implying a smaller resonant annihilation cross section.

section the relic density bound becomes very constraining. The structures along the line $M_{Z'} \approx m_\chi$ in fig. 5 can be understood from the appearance of the $\chi\chi \rightarrow Z'Z'$ annihilation channel in that region which lead to a different dependence of $\sigma_{\chi\chi}v$ on g_χ and g_q . As can be seen in fig. 5 the results for $g_\chi = g_q$ and $g_\chi = 10 g_q$ differ significantly in this region.

Finally, we have investigated the impact of a subdominant dark matter species. As expected, the precise value of Ω_χ generically has only a minor impact on the bound. Numerically, the bound changes by less than 20% for $\Omega_\chi/\Omega_{\text{tot}} > 0.1$ and by less than a factor of two as long as $\Omega_\chi/\Omega_{\text{tot}} > 0.01$. An even smaller relic density can typically only be achieved if the coupling constants $g_{\chi,q}$, and consequently $\Gamma_{Z'}$, are large. The relation between $\langle\sigma_{\chi\chi}v\rangle$ and σ_{SD} is more complicated in this case and $\Omega_\chi \sigma_{\text{SD}}$ exhibits a non-trivial scaling behavior.

7 Discussion and conclusions

We have derived lower bounds on the product of the DM–nucleus scattering cross section and the local DM density from a positive signal in a direct detection experiment, which is independent of the DM velocity distribution. If an upper bound on the local DM density from kinematical Milky Way observations is applied, our bounds provide a robust lower bound on the scattering cross section.

We have discussed different versions of such bounds. One of them is based only on the number of events observed in a certain recoil energy interval and leads to a robust bound even in the case of few signal events. As illustration we have applied this bound in the context of the 3 candidate events found in CDMS silicon data. A second version requires an accurate measurement of the recoil spectrum, including a deconvolution of resolution and efficiency factors, however, it provides more stringent lower bounds on the cross section.

In this work we have restricted the analysis to time-averaged signals in direct detection experiments, neglecting the small annual modulation effect. In ref. [29] it is shown that also the annual modulation signal can be used to obtain a halo-independent lower bound on the scattering cross section, in particular in combination with the methods developed in refs. [14, 15].

In order to illustrate our bounds we have assumed the observation of a signal in just one direct detection experiment. Let us briefly comment on the case of a positive signal in more than one experiment, using different target nuclei. A priori our bound can be calculated for each experiment and it may happen that depending on the DM mass different experiments provide the strongest bound. However, in the lucky case of a multiple DM detection, more information is available and other methods may be more appropriate. First, one may try to answer the question of whether the signals are consistent with each other in a halo-independent way [7–27]. Assuming that they are consistent, the methods of ref. [8] can be used to extract the DM mass in a halo-independent way, see also [27]. This DM mass can then be used for the bounds on the cross section discussed here. Finally, more information on particle physics can be obtained. For instance one can try to infer the relative coupling strength to neutrons

and protons from the data simultaneously to bounding the cross section. A detailed investigation of the multi-detection case is beyond the scope of this work.

For a given particle physics model, a lower bound on the scattering cross section from direct detection data can be compared to data from LHC. As an example we consider a so-called simplified DM model and derive allowed regions in the model parameter space by the comparison of an assumed signal in a future direct detection experiment with upper limits from LHC mono-jet searches.

Finally we have shown how our bounds from a direct detection signal can be used to test the hypothesis that the particle responsible for the signal is a thermal relic. Furthermore, the bound can be used to formulate a condition which has to be fulfilled under the assumption of a thermal history of the DM candidate, irrespective of whether this particle provides all of the DM or only part of it. Again we have used a simplified DM model as an example, and have identified the region in the space of DM and mediator masses, which would exclude the thermal freeze-out mechanism for an assumed direct detection signal.

While in this work we have used a simple DM model consisting of a Majorana fermion as DM interacting with the Standard Model via a Z' mediator, we note that our bounds can be applied for any other model which allows to relate the scattering cross section to LHC observables and the relic abundance. In our example model all observables depend only on four parameters (DM and mediator masses and two couplings), in large part of the parameter space only on three (only the product of the two couplings is relevant). In more complicated models with more parameters a marginalization over some parameters (or optimization of the inequalities) will have to be performed.

In the same way we used our halo bounds for the comparison of a direct detection signal with LHC limits, it is also possible to confront a direct detection signal with limits from indirect detection (searching for DM annihilation products from astrophysical environments like dwarf galaxies or the galactic centre). For the specific Z' model used as an example in this work, the annihilation cross section $\langle\sigma v\rangle$ is dominated by p -wave processes and, consequently, the annihilation rate today is strongly suppressed. Therefore, we expect limits from indirect detection to be very weak for this model.

To conclude, we want to encourage the community to show the DM direct detection positive results, which hopefully will occur at some point in the near future, using the velocity distribution independent lower bound on the cross section derived here, in addition to the usually assumed Maxwellian halo model.

Note added: After the completion of this work and submission to the arXiv, the preprint ref. [75] appeared, where also a halo-independent lower bound on the scattering cross section is derived.

Acknowledgements: We would like to thank Felix Kahlhoefer for helpful discussions. The work of MB was partially supported by the Göran Gustafsson Foundation. TS and SV acknowledge support from the European Union FP7 ITN INVISIBLES (Marie Curie Actions, PITN-GA-2011-289442).

References

- [1] M. W. Goodman and E. Witten, *Detectability of Certain Dark Matter Candidates*, *Phys.Rev.* **D31** (1985) 3059.
- [2] A. Drukier, K. Freese, and D. Spergel, *Detecting Cold Dark Matter Candidates*, *Phys.Rev.* **D33** (1986) 3495–3508.
- [3] K. Freese, J. A. Frieman, and A. Gould, *Signal Modulation in Cold Dark Matter Detection*, *Phys. Rev.* **D37** (1988) 3388.
- [4] M. Vogelsberger, A. Helmi, V. Springel, S. D. White, J. Wang, et al., *Phase-space structure in the local dark matter distribution and its signature in direct detection experiments*, *Mon.Not.Roy.Astron.Soc.* **395** (2009) 797–811, [[arXiv:0812.0362](#)].
- [5] M. Kuhlen, N. Weiner, J. Diemand, P. Madau, B. Moore, et al., *Dark Matter Direct Detection with Non-Maxwellian Velocity Structure*, *JCAP* **1002** (2010) 030, [[arXiv:0912.2358](#)].
- [6] M. Kuhlen, M. Lisanti, and D. N. Spergel, *Direct Detection of Dark Matter Debris Flows*, *Phys.Rev.* **D86** (2012) 063505, [[arXiv:1202.0007](#)].
- [7] M. Drees and C.-L. Shan, *Reconstructing the Velocity Distribution of WIMPs from Direct Dark Matter Detection Data*, *JCAP* **0706** (2007) 011, [[astro-ph/0703651](#)].
- [8] M. Drees and C.-L. Shan, *Model-Independent Determination of the WIMP Mass from Direct Dark Matter Detection Data*, *JCAP* **0806** (2008) 012, [[arXiv:0803.4477](#)].
- [9] P. J. Fox, J. Liu, and N. Weiner, *Integrating Out Astrophysical Uncertainties*, *Phys.Rev.* **D83** (2011) 103514, [[arXiv:1011.1915](#)].
- [10] P. J. Fox, G. D. Kribs, and T. M. Tait, *Interpreting Dark Matter Direct Detection Independently of the Local Velocity and Density Distribution*, *Phys.Rev.* **D83** (2011) 034007, [[arXiv:1011.1910](#)].
- [11] C. McCabe, *DAMA and CoGeNT without astrophysical uncertainties*, *Phys.Rev.* **D84** (2011) 043525, [[arXiv:1107.0741](#)].
- [12] C. McCabe, *The Astrophysical Uncertainties Of Dark Matter Direct Detection Experiments*, *Phys. Rev.* **D82** (2010) 023530, [[arXiv:1005.0579](#)].
- [13] M. T. Frandsen, F. Kahlhoefer, C. McCabe, S. Sarkar, and K. Schmidt-Hoberg, *Resolving astrophysical uncertainties in dark matter direct detection*, *JCAP* **1201** (2012) 024, [[arXiv:1111.0292](#)].
- [14] J. Herrero-Garcia, T. Schwetz, and J. Zupan, *On the annual modulation signal in dark matter direct detection*, *JCAP* **1203** (2012) 005, [[arXiv:1112.1627](#)].
- [15] J. Herrero-Garcia, T. Schwetz, and J. Zupan, *Astrophysics independent bounds on the annual modulation of dark matter signals*, *Phys.Rev.Lett.* **109** (2012) 141301, [[arXiv:1205.0134](#)].
- [16] E. Del Nobile, G. B. Gelmini, P. Gondolo, and J.-H. Huh, *Halo-independent analysis of direct detection data for light WIMPs*, *JCAP* **1310** (2013) 026, [[arXiv:1304.6183](#)].
- [17] E. Del Nobile, G. Gelmini, P. Gondolo, and J.-H. Huh, *Generalized Halo Independent Comparison of Direct Dark Matter Detection Data*, *JCAP* **1310** (2013) 048,

- [arXiv:1306.5273].
- [18] N. Bozorgnia, J. Herrero-Garcia, T. Schwetz, and J. Zupan, *Halo-independent methods for inelastic dark matter scattering*, *JCAP* **1307** (2013) 049, [arXiv:1305.3575].
 - [19] J. F. Cherry, M. T. Frandsen, and I. M. Shoemaker, *Halo Independent Direct Detection of Momentum-Dependent Dark Matter*, *JCAP* **1410** (2014), no. 10 022, [arXiv:1405.1420].
 - [20] P. J. Fox, Y. Kahn, and M. McCullough, *Taking Halo-Independent Dark Matter Methods Out of the Bin*, *JCAP* **1410** (2014), no. 10 076, [arXiv:1403.6830].
 - [21] B. Feldstein and F. Kahlhoefer, *A new halo-independent approach to dark matter direct detection analysis*, *JCAP* **1408** (2014) 065, [arXiv:1403.4606].
 - [22] B. Feldstein and F. Kahlhoefer, *Quantifying (dis)agreement between direct detection experiments in a halo-independent way*, *JCAP* **1412** (2014), no. 12 052, [arXiv:1409.5446].
 - [23] N. Bozorgnia and T. Schwetz, *What is the probability that direct detection experiments have observed Dark Matter?*, *JCAP* **1412** (2014), no. 12 015, [arXiv:1410.6160].
 - [24] A. J. Anderson, P. J. Fox, Y. Kahn, and M. McCullough, *Halo-Independent Direct Detection Analyses Without Mass Assumptions*, [arXiv:1504.03333].
 - [25] S. Scopel and K. Yoon, *A systematic halo-independent analysis of direct detection data within the framework of Inelastic Dark Matter*, *JCAP* **1408** (2014) 060, [arXiv:1405.0364].
 - [26] B. J. Kavanagh and A. M. Green, *Improved determination of the WIMP mass from direct detection data*, *Phys.Rev.* **D86** (2012) 065027, [arXiv:1207.2039].
 - [27] B. J. Kavanagh and A. M. Green, *Model independent determination of the dark matter mass from direct detection experiments*, *Phys.Rev.Lett.* **111** (2013), no. 3 031302, [arXiv:1303.6868].
 - [28] M. Blennow, J. Herrero-Garcia, and T. Schwetz, *A halo-independent lower bound on the dark matter capture rate in the Sun from a direct detection signal*, [arXiv:1502.03342].
 - [29] J. Herrero-Garcia, *Halo-independent tests of dark matter annual modulation signals*, [arXiv:1506.03503].
 - [30] J. Lavalle and S. Magni, *Making sense of the local Galactic escape speed estimates in direct dark matter searches*, *Phys.Rev.* **D91** (2015) 023510, [arXiv:1411.1325].
 - [31] **CDMS Collaboration** Collaboration, R. Agnese et al., *Silicon Detector Dark Matter Results from the Final Exposure of CDMS II*, *Phys.Rev.Lett.* **111** (2013), no. 25 251301, [arXiv:1304.4279].
 - [32] **CDMS Collaboration**, **EDELWEISS Collaboration** Collaboration, Z. Ahmed et al., *Combined Limits on WIMPs from the CDMS and EDELWEISS Experiments*, *Phys.Rev.* **D84** (2011) 011102, [arXiv:1105.3377].
 - [33] **XENON100 Collaboration** Collaboration, E. Aprile et al., *Dark Matter Results from 225 Live Days of XENON100 Data*, *Phys.Rev.Lett.* **109** (2012) 181301, [arXiv:1207.5988].

- [34] **LUX Collaboration** Collaboration, D. Akerib et al., *First results from the LUX dark matter experiment at the Sanford Underground Research Facility*, *Phys.Rev.Lett.* **112** (2014), no. 9 091303, [[arXiv:1310.8214](#)].
- [35] **CRESST-II Collaboration** Collaboration, G. Angloher et al., *Results on low mass WIMPs using an upgraded CRESST-II detector*, *Eur.Phys.J.* **C74** (2014), no. 12 3184, [[arXiv:1407.3146](#)].
- [36] **SuperCDMS Collaboration** Collaboration, R. Agnese et al., *Search for Low-Mass Weakly Interacting Massive Particles with SuperCDMS*, *Phys.Rev.Lett.* **112** (2014), no. 24 241302, [[arXiv:1402.7137](#)].
- [37] X. Xiao, X. Chen, A. Tan, Y. Chen, X. Cui, et al., *Low-mass dark matter search results from full exposure of PandaX-I experiment*, [arXiv:1505.00771](#).
- [38] K. A. McCarthy, “Dark matter search results from the silicon detectors of the cryogenic dark matter search experiment.” Presented at the APS Physics Meeting, Denver, Colorado, 2013.
- [39] P. Salucci, F. Nesti, G. Gentile, and C. Martins, *The dark matter density at the Sun’s location*, *Astron.Astrophys.* **523** (2010) A83, [[arXiv:1003.3101](#)].
- [40] S. Garbari, C. Liu, J. I. Read, and G. Lake, *A new determination of the local dark matter density from the kinematics of K dwarfs*, *Mon.Not.Roy.Astron.Soc.* **425** (2012) 1445, [[arXiv:1206.0015](#)].
- [41] L. Zhang, H.-W. Rix, G. van de Ven, J. Bovy, C. Liu, et al., *The Gravitational Potential Near the Sun From SEGUE K-dwarf Kinematics*, *Astrophys.J.* **772** (2013) 108, [[arXiv:1209.0256](#)].
- [42] R. Catena and P. Ullio, *A novel determination of the local dark matter density*, *JCAP* **1008** (2010) 004, [[arXiv:0907.0018](#)].
- [43] M. Weber and W. de Boer, *Determination of the Local Dark Matter Density in our Galaxy*, *Astron.Astrophys.* **509** (2010) A25, [[arXiv:0910.4272](#)].
- [44] P. J. McMillan, *Mass models of the Milky Way*, *Mon.Not.Roy.Astron.Soc.* **414** (2011) 2446–2457, [[arXiv:1102.4340](#)].
- [45] F. Iocco, M. Pato, G. Bertone, and P. Jetzer, *Dark Matter distribution in the Milky Way: microlensing and dynamical constraints*, *JCAP* **1111** (2011) 029, [[arXiv:1107.5810](#)].
- [46] M. Pato, F. Iocco, and G. Bertone, *Dynamical constraints on the dark matter distribution in the Milky Way*, [arXiv:1504.06324](#).
- [47] J. Read, *The Local Dark Matter Density*, *J.Phys.* **G41** (2014) 063101, [[arXiv:1404.1938](#)].
- [48] **XENON100 Collaboration**, E. Aprile et al., *Limits on spin-dependent WIMP-nucleon cross sections from 225 live days of XENON100 data*, *Phys.Rev.Lett.* **111** (2013), no. 2 021301, [[arXiv:1301.6620](#)].
- [49] C. Savage, A. Scaffidi, M. White, and A. G. Williams, *LUX likelihood and limits on spin-independent and spin-dependent WIMP couplings with LUXCalc*, [arXiv:1502.02667](#).

- [50] **SIMPLE** Collaboration, M. Felizardo et al., *The SIMPLE Phase II Dark Matter Search*, *Phys.Rev.* **D89** (2014), no. 7 072013, [[arXiv:1404.4309](#)].
- [51] **Super-Kamiokande** Collaboration, K. Choi et al., *Search for neutrinos from annihilation of captured low-mass dark matter particles in the Sun by Super-Kamiokande*, [arXiv:1503.04858](#).
- [52] **IceCube collaboration** Collaboration, M. Aartsen et al., *Search for dark matter annihilations in the Sun with the 79-string IceCube detector*, *Phys.Rev.Lett.* **110** (2013), no. 13 131302, [[arXiv:1212.4097](#)].
- [53] V. Bednyakov and F. Simkovic, *Nuclear spin structure in dark matter search: The Finite momentum transfer limit*, *Phys.Part.Nucl.* **37** (2006) S106–S128, [[hep-ph/0608097](#)].
- [54] D. Malling, D. Akerib, H. Araujo, X. Bai, S. Bedikian, et al., *After LUX: The LZ Program*, [arXiv:1110.0103](#).
- [55] **DARWIN Consortium** Collaboration, L. Baudis, *DARWIN: dark matter WIMP search with noble liquids*, *J.Phys.Conf.Ser.* **375** (2012) 012028, [[arXiv:1201.2402](#)].
- [56] **XENON1T collaboration** Collaboration, E. Aprile, *The XENON1T Dark Matter Search Experiment*, *Springer Proc.Phys.* **C12-02-22** (2013) 93–96, [[arXiv:1206.6288](#)].
- [57] J. Abdallah, A. Ashkenazi, A. Boveia, G. Busoni, A. De Simone, et al., *Simplified Models for Dark Matter and Missing Energy Searches at the LHC*, [arXiv:1409.2893](#).
- [58] S. Malik, C. McCabe, H. Araujo, A. Belyaev, C. Boehm, et al., *Interplay and Characterization of Dark Matter Searches at Colliders and in Direct Detection Experiments*, [arXiv:1409.4075](#).
- [59] M. Chala, F. Kahlhoefer, M. McCullough, G. Nardini, and K. Schmidt-Hoberg, *Constraining Dark Sectors with Monojets and Dijets*, [arXiv:1503.05916](#).
- [60] G. Arcadi, Y. Mambrini, M. H. G. Tytgat, and B. Zaldivar, *Invisible Z' and dark matter: LHC vs LUX constraints*, *JHEP* **1403** (2014) 134, [[arXiv:1401.0221](#)].
- [61] O. Lebedev and Y. Mambrini, *Axial dark matter: The case for an invisible Z* , *Phys.Lett.* **B734** (2014) 350–353, [[arXiv:1403.4837](#)].
- [62] M. Duerr and P. Fileviez Perez, *Theory for Baryon Number and Dark Matter at the LHC*, *Phys.Rev.* **D91** (2015), no. 9 095001, [[arXiv:1409.8165](#)].
- [63] O. Buchmueller, M. J. Dolan, S. A. Malik, and C. McCabe, *Characterising dark matter searches at colliders and direct detection experiments: Vector mediators*, *JHEP* **1501** (2015) 037, [[arXiv:1407.8257](#)].
- [64] G. Belanger, F. Boudjema, A. Pukhov, and A. Semenov, *Dark matter direct detection rate in a generic model with micrOMEGAs 2.2*, *Comput.Phys.Commun.* **180** (2009) 747–767, [[arXiv:0803.2360](#)].
- [65] **ATLAS** Collaboration, G. Aad et al., *Search for new phenomena in final states with an energetic jet and large missing transverse momentum in pp collisions at $\sqrt{s} = 8$ TeV with the ATLAS detector*, [arXiv:1502.01518](#).
- [66] **CMS** Collaboration, V. Khachatryan et al., *Search for dark matter, extra dimensions, and unparticles in monojet events in proton-proton collisions at $\sqrt{s} = 8$ TeV*,

- [arXiv:1408.3583](#).
- [67] A. Belyaev, N. D. Christensen, and A. Pukhov, *CalcHEP 3.4 for collider physics within and beyond the Standard Model*, *Comput.Phys.Commun.* **184** (2013) 1729–1769, [[arXiv:1207.6082](#)].
 - [68] T. Sjostrand, S. Mrenna, and P. Z. Skands, *A Brief Introduction to PYTHIA 8.1*, *Comput.Phys.Commun.* **178** (2008) 852–867, [[arXiv:0710.3820](#)].
 - [69] **DELPHES 3** Collaboration, J. de Favereau et al., *DELPHES 3, A modular framework for fast simulation of a generic collider experiment*, *JHEP* **1402** (2014) 057, [[arXiv:1307.6346](#)].
 - [70] *Sensitivity to WIMP Dark Matter in the Final States Containing Jets and Missing Transverse Momentum with the ATLAS Detector at 14 TeV LHC*, Tech. Rep. ATL-PHYS-PUB-2014-007, CERN, Geneva, Jun, 2014.
 - [71] G. Belanger, F. Boudjema, A. Pukhov, and A. Semenov, *micrOMEGAs3: A program for calculating dark matter observables*, *Comput.Phys.Commun.* **185** (2014) 960–985, [[arXiv:1305.0237](#)].
 - [72] **Planck** Collaboration, P. Ade et al., *Planck 2015 results. XIII. Cosmological parameters*, [arXiv:1502.01589](#).
 - [73] D. Anderhalden, J. Diemand, G. Bertone, A. V. Maccio, and A. Schneider, *The Galactic Halo in Mixed Dark Matter Cosmologies*, *JCAP* **1210** (2012) 047, [[arXiv:1206.3788](#)].
 - [74] G. Bertone, D. G. Cerdeno, M. Fornasa, R. R. de Austri, and R. Trotta, *Identification of Dark Matter particles with LHC and direct detection data*, *Phys.Rev.* **D82** (2010) 055008, [[arXiv:1005.4280](#)].
 - [75] F. Ferrer, A. Ibarra, and S. Wild, *A novel approach to derive halo-independent limits on dark matter properties*, [arXiv:1506.03386](#).